Macromolecules

ARTICLE

pubs.acs.org/Macromolecules

FT-IR Image Processing Algorithms for In-Plane Orientation Function and Azimuth Angle of Uniaxially Drawn Polyethylene Composite Film

Yuta Hikima, Junko Morikawa,* and Toshimasa Hashimoto

Tokyo Institute of Technology, 2-12-1, Meguro-ku, Tokyo 152-8550, Japan

ABSTRACT: The FT-IR imaging method has been applied to acquire thousands of infrared spectra at a spatial resolution near the diffraction limit using an IR image sensor. We propose the mathematical procedure to visualize the degree of molecular orientation and the azimuth angle of the orientation axis using the polarized absorbance images measured with a linear polarizer settled at four different angles. It mathematically synthesizes in-plane orientation function that is independent of the direction of the incident polarization and visualizes the molecular orientation and the azimuth angle using an IR imaging sensor. By introducing the azimuth angle image, a small change of the molecular orientation can be detected visually in the early stage of local deformation of the uniaxially drawn process of the polyethylene composite film.

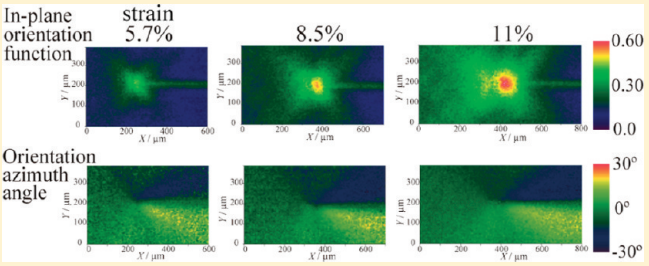

INTRODUCTION

The Fourier transform infrared spectroscopic imaging (FT-IR imaging) method enables "chemical imaging" by combining the spectral and spatial information. The apparatus of FT-IR imaging usually consists of an infrared microscope, a step-scan spectrometer, and a focal plane array (FPA) with a photoconductive sensor of mercury cadmium telluride (HgCdTe (MCT)).[1,2] This method renders images consisting of chemical information from all pixels covering the measuring areas at the same time, and thousands of infrared spectra can be acquired at a spatial resolution near to the diffraction limit in a few minutes.[1,2] A linear sensor can also perform FT-IR imaging by a raster scanning.[3]

FT-IR imaging method has been applied to various samples. Koenig et al. investigated the polymer dissolution process,[4−8] the polymer dispersed liquid crystals,[9−11] and nematic liquid crystals.[12] The interface of fiber/epoxy composites,[13,14] the polymerization process of hydrogel,[15−17] the phase separate from polymer blends systems,[18−21] the cross section of multilayer films,[21,22] the crystallinity distribution of injection-molded films,[23] and the material distribution near the surface of self-stratified film[24] were visualized by the FT-IR imaging method. Furthermore, the attenuated total reflection (ATR)-FT-IR imaging method with a FPA[25,26] or a linear array[27] sensor has been reported since a decade ago. The spatial resolution of ATR-FT-IR imaging method is higher than the transmission method of FT-IR imaging because the ATR crystal has a higher refractive index.[28,29] Kazarian et al. applied this method to the polymer films processed under the high-pressure or supercritical CO_2,[30−32] and the dissolution process of drugs.[33−35]

On the other hand, the infrared spectroscopy measured with a polarized incident light can estimate the molecular orientation in the anisotropic materials using the infrared dichroism.[36,37] The dichroic ratio and the Hermans orientation function are usually used for the quantitative analysis of molecular orientation.[44−46] Therefore, FT-IR imaging combined with a linear polarized incident light offers a possibility to visualize the anisotropic distribution and the chemical information, simultaneously. Vogel et al. reported that the distribution of molecular orientation with chemical information in uniaxially drawn polymer films.[18,19,38,39] Several groups investigated anisotropic polymer samples by FT-IR imaging, such as spherulites,[40−42] the laminated film,[3] the cross section of the carbonated drink bottle,[21] and the epoxy resins filled with particles.[43] However, the analytic method using a pair of orthogonal polarizations is not always suitable to visualize the degree of molecular orientation because the dichroic ratio and Hermans orientation function depend on the direction of the incident linear polarization, as is seen in the apparently nonorientation areas in a PCL (poly-ε-caprolactone) spherulite.[41]

We propose the mathematical procedure to visualize the degree of molecular orientation and the azimuth angle of the orientation axis using the polarized absorbance images measured with a linear polarizer settled at four different angles. It mathematically synthesizes in-plane orientation function that is independent of the direction of the incident linear polarization. The local deformation of the uniaxially drawn fiber composite film is visualized with the magnitude image of the orientation function and the azimuth angle image of the orientation axis.

EXPERIMENTAL SECTION

The single ultrahigh molecular weight polyethylene (PE) fiber (Dyneema, Toyobo Co., Ltd.) was put between the low-density polyethylene (LDPE; grade: 68, Mitsui Chemicals) films and hot pressed at 125 °C. The LDPE/PE fiber composite film was sized 20 μm

Received: February 14, 2011
Revised: April 14, 2011
Published: April 29, 2011

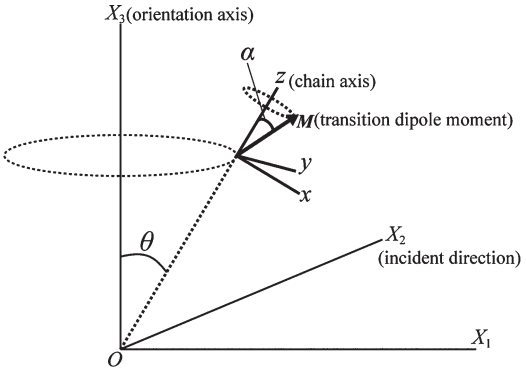

Figure 1. Schematic diagram of the axes $O-X_1X_2X_3$ relative to the orientation distribution of the chain axis z and the axes $O-xyz$ relative to the orientation distribution of transition dipole moment **M** within a uniaxially oriented sample.

thickness, 15 mm long and 8 mm wide. The LDPE/PE fiber composite film was uniaxially drawn by a miniaturized stretching machine at the strain rate of 1%/s.

The Fourier transform infrared spectroscopic imaging (FT-IR imaging) method was performed by using Spectrum Spotlight 300 (PerkinElmer Inc.), which consists of Fourier transform infrared spectrometer (Spectrum One, PerkinElmer Inc.), an infrared microscope, the automatic X-Y-Z stage with a sample holder, and mercury cadmium telluride (MCT) detectors aligned as an array of 16 × 1 device. The sample is put on the stage with applying certain tensile strains, and infrared absorption images around the fiber end in the LDPE/PE fiber composite film were obtained by a raster scanning in X-Y directions. Infrared spectra was measured with transmission mode, 4000−650 cm^{-1} spectral region, 4 cm^{-1} spectral resolution, and 16 scans. The imaging pixel size is 6.25 μm × 6.25 μm. In order to produce the image with a polarized irradiation, a gold wire-grid polarizer was mounted between the sample and the detector. The drawing direction was set corresponding to the polarizer angle 0°. In order to remove the influence of baseline fluctuation, the absorption bands in all spectra are corrected by the subtraction of baseline before calculating the molecular orientation.

MATHEMATICAL PROCEDURE

In order to obtain the degree of molecular orientation by infrared spectroscopy, the measurement with a pair of orthogonal polarizations is usually performed.[44−46] Here, these polarizations are called as the "parallel polarization" and "perpendicular polarization". The dichroic ratio D is defined as

$$D = \frac{A_{\parallel}}{A_{\perp}} \tag{1}$$

where $A_{\parallel}$ and $A_{\perp}$ are the absorbance measured under a parallel and a perpendicular polarization, respectively. The second moment of orientation distribution function, which is called "Hermans orientation function" f, is related to the dichroic ratio[44,45]

$$f = \frac{3\langle\cos^2\theta\rangle - 1}{2} = \frac{D-1}{D+2}\frac{2}{3\cos^2\alpha - 1} \tag{2}$$

where θ is the angle between the orientation axis X_3 and the chain axis z and α is the angle between the chain axis z and the transition dipole moment **M** (shown in Figure 1). The angle α is unique to each absorbance band, and if α is smaller than $(1/\sqrt{3})$ ($\cong$54.73°), it is defined as a parallel band, and if it is larger, it is a perpendicular band.[45,46] In the case of uniaxially oriented

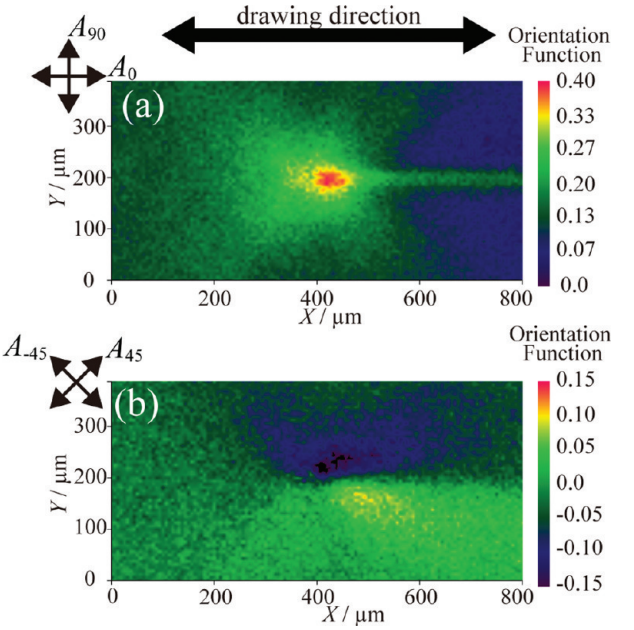

Figure 2. FT-IR imaging results of Hermans orientation function calculated at 720 cm^{-1} from eqs 1 and 2 with absorbance images measured with a pair of linear polarizer angles (a) 0° and 90° and (b) +45° and −45°, respectively, applied to a polyethylene fiber composite film (a PE fiber, Dyneema, embedded in LDPE matrix) with 11% tensile strain.

samples, the polarizations parallel and perpendicular to the orientation axis are adopted to calculate dichroic ratio and Hermans orientation function. The range of dichroic ratio and Hermans orientation function are allowed from 0 to ∞ and −0.5 to 1, respectively. When the parallel polarization corresponds perfectly to the orientation axis, Hermans orientation function exhibits the maximum value, but if imperfectly, the obtained value will be smaller. For example, if the direction of parallel polarization forms 45° with the orientation axis, Hermans orientation function will exhibit 0; in other words, the anisotropic sample is apparently detected as isotropic. It sometimes causes a serious misunderstanding when the molecular orientation is visualized by using FT-IR imaging method as indicated below.

Figure 2 shows the distribution of Hermans orientation function at 720 cm^{-1} calculated from two pairs of the orthogonal polarized absorbances: (a) A_0 and A_{90} and (b) A_{+45} and A_{-45} using eqs 1 and 2 near the fiber end in the LDPE/PE fiber composite sample at 11% tensile strain. Here, we assume that $A_{\parallel} = A_0$ in Figure 2a and $A_{\parallel} = A_{+45}$ in Figure 2b, respectively. The value of each pixel is expressed as the false color image with a color bar at the right side. The calculated imaging results in Figure 2 obviously visualize the different patterns of orientation function, in which the molecular orientation in the direction inclining ±45° from the drawing direction is not clearly observed in Figure 2a, and vice versa in Figure 2b. It indicates that Hermans orientation function does not fix the magnitude image of in-plane molecular orientation when it is determined only with a pair of orthogonal polarized absorbance.

In order to define the degree of in-plane molecular orientation by the FT-IR imaging method, the direction of orientation axis (X_3 in Figure 1) in the sample plane must be determined at each pixel. Here, we introduce the mathematical algorithm in order to determine the "in-plane orientation function" for the estimation

of the degree of in-plane molecular orientation, which is independent of the direction of the incident linear polarization. Moreover, the "orientation azimuth angle" for estimation of the azimuth of orientation axis X_3 in the sample plane is introduced, which expresses the polarizer angle when the incident polarized radiation is parallel to the orientation axis. A pair of "in-plane orientation function" and "orientation azimuth angle" can be determined from four different absorbance measured under two pairs of orthogonal polarized incident radiation that has passed through a linear polarizer settled at four different directions.

From the principles of spectroscopy, it can be shown that the absorbance A of polarized radiation is proportional to the square of the dot product of the electric vector of the polarized ray, **p**, with transition moment vector **M** for particular vibration:

$$A \propto (\mathbf{p}\cdot\mathbf{M})^2 = (pM\cos\mu)^2 \tag{3}$$

where μ is the angle between **M** and **p**. The projection of **M** onto the X_1-X_3 plane is considered and decomposed into the components parallel to X_1 and X_3 (the coordinate is shown in Figure 1). In fact, the absorbance measured under polarized radiation corresponds to the total sum of absorbance for all transition moments within the measurement area. If the polarization is parallel to the orientation axis (X_3), the maximum or minimum absorbance will be obtained at parallel or perpendicular band, respectively. This relationship is expressed by

$$A_\gamma = A_{\max}\cos^2(\gamma-\psi) + A_{\min}\sin^2(\gamma-\psi) \tag{4}$$

where γ is the polarizer angle, $A_{\max}$ and $A_{\min}$ are the maximum and minimum absorbance, respectively, and ψ is the polarizer angle when $A = A_{\max}$.[36] The relationship expressed by eq 4 is shown in Figure 3. Equation 4 can be transformed into

$$A_\gamma = \frac{A_{\max}+A_{\min}}{2} + \frac{A_{\max}-A_{\min}}{2}\cos 2(\gamma-\psi) \tag{5}$$

Substituting four particular polarizer angles $\gamma = 0°$, $+45°$, $-45°$, and $90°$ into eq 5 and absorbance, A_0, A_{+45}, A_{-45}, and A_{90} can be derived as

$$\begin{aligned} A_0 &= \frac{A_{\max}+A_{\min}}{2} + \frac{A_{\max}-A_{\min}}{2}\cos 2\psi \\ A_{90} &= \frac{A_{\max}+A_{\min}}{2} - \frac{A_{\max}-A_{\min}}{2}\cos 2\psi \\ A_{+45} &= \frac{A_{\max}+A_{\min}}{2} + \frac{A_{\max}-A_{\min}}{2}\sin 2\psi \\ A_{-45} &= \frac{A_{\max}+A_{\min}}{2} - \frac{A_{\max}-A_{\min}}{2}\sin 2\psi \end{aligned} \tag{6}$$

In order to eliminate the first term of each equation, the following two variables are introduced:

$$\begin{aligned} a &\equiv A_0 - A_{90} \\ b &\equiv A_{+45} - A_{-45} \end{aligned} \tag{7}$$

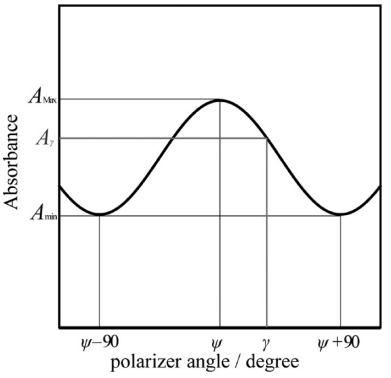

Figure 3. Schematic depiction of IR absorbance dependent on the angle of a linear polarizer, as derived in eq 4, in the uniaxially oriented sample.

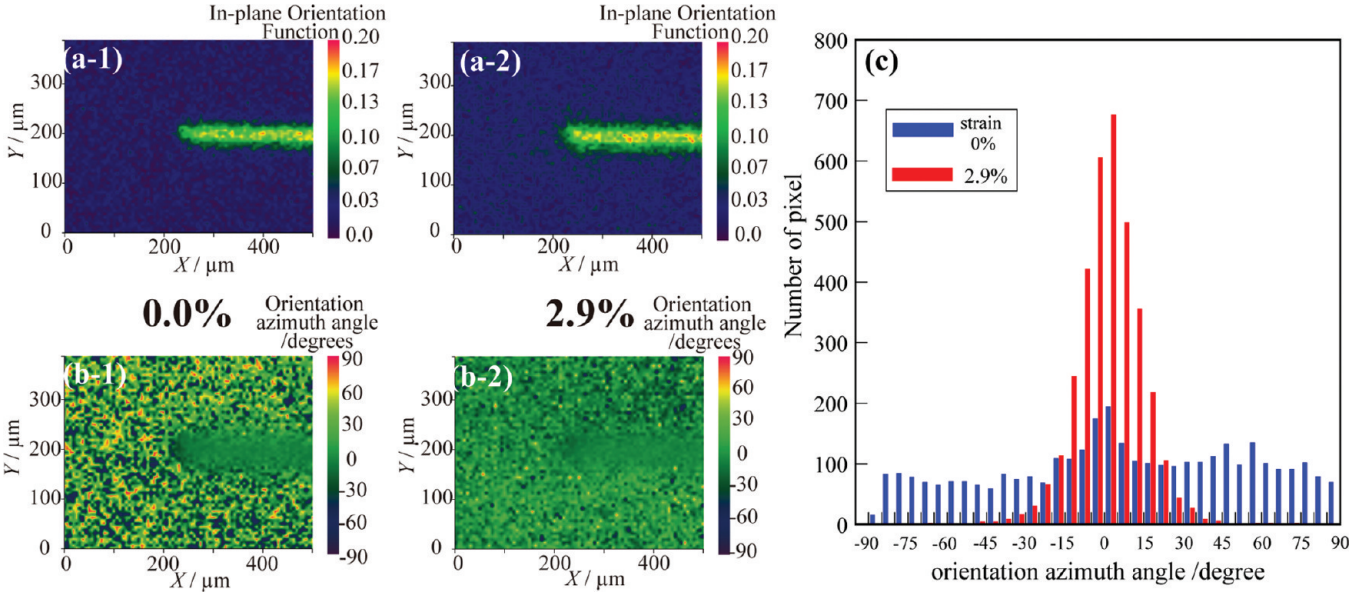

Figure 4. FT-IR imaging results of (a) in-plane orientation function, (b) orientation azimuth angle calculated at 720 cm^{-1} in the polyethylene fiber composite film at 0% and 2.9% tensile strain, and (c) the image histogram of orientation azimuth angle images calculated from (b-1) with blue bars and (b-2) with red ones.

dx.doi.org/10.1021/ma2003129 |*Macromolecules* 2011, 44, 3950–3957

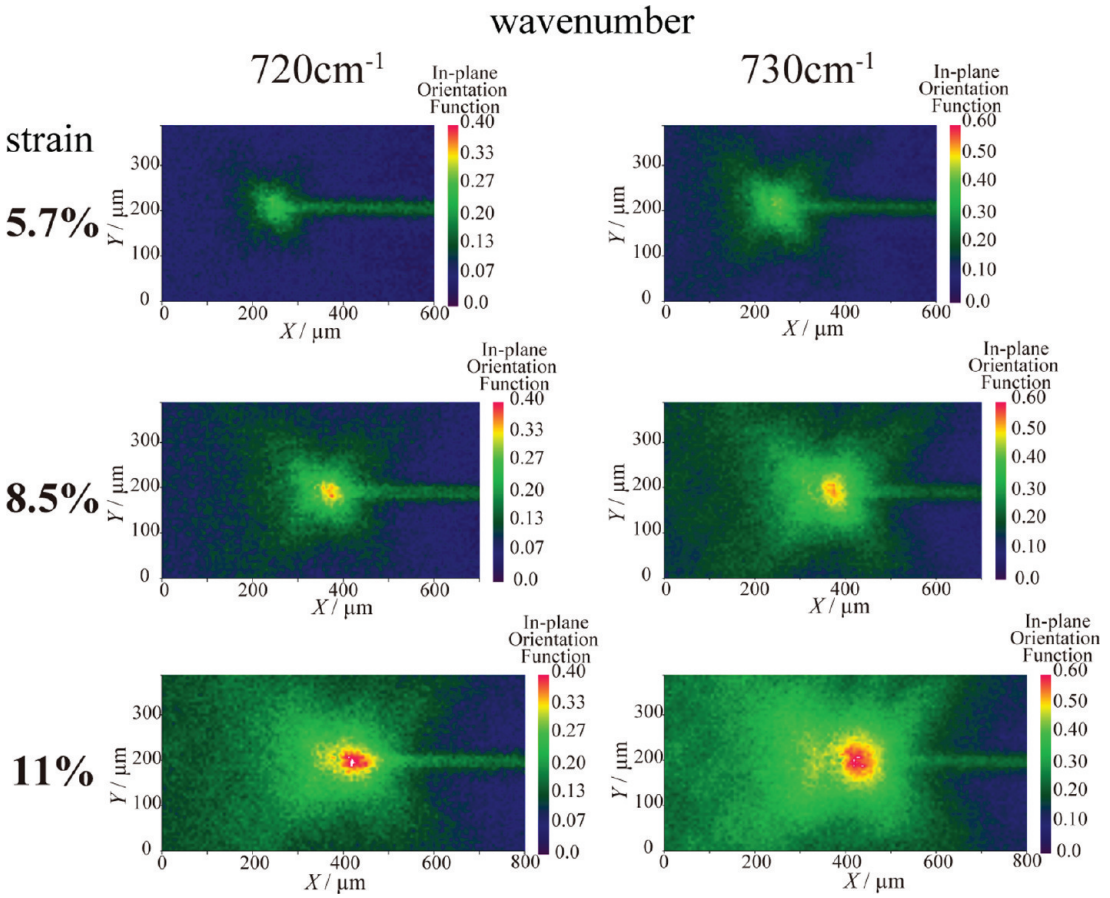

Figure 5. Magnitude images of in-plane orientation function calculated at (left) 720 and (right) 730 cm^{-1} in the polyethylene fiber composite film at (upper) 5.7, (middle) 8.5, and (lower) 11% tensile strain.

From here we find expressions for the maximum dichroic difference $A_{max} - A_{min}$ and the angle ψ:

$$A_{max} - A_{min} = \sqrt{a^2 + b^2} \tag{8}$$

$$\psi = \frac{1}{2}\tan^{-1}\left(\frac{b}{a}\right) \tag{9}$$

For the calculation of maximum and minimum dichroic ratios, D_{max} and D_{min}, respectively, following the variable c is introduced:

$$c \equiv \frac{A_0 + A_{90} + A_{+45} + A_{-45}}{2} (\cong A_{max} + A_{min}) \tag{10}$$

Then, the maximum and the minimum dichroic ratios can be found as

$$D_{max} = \frac{c + \sqrt{a^2 + b^2}}{c - \sqrt{a^2 + b^2}} \tag{11}$$

$$D_{min} = \frac{c - \sqrt{a^2 + b^2}}{c + \sqrt{a^2 + b^2}} \tag{12}$$

When the incident polarization is parallel to the orientation axis, the maximum or the minimum absorbance is obtained with the parallel or perpendicular band, respectively. Therefore, in the case of parallel band, the in-plane orientation function, f_Ψ, is calculated from D_{max}, and the orientation azimuth angle, Ψ, corresponds to ψ

$$f_\Psi = \frac{D_{max} - 1}{D_{max} + 2}\frac{2}{3\cos^2\alpha - 1} \qquad \Psi = \psi \tag{13a}$$

In the case of the perpendicular band, f_Ψ is calculated from D_{min} and Ψ corresponds to $\psi + 90°$:

$$f_\Psi = \frac{D_{min} - 1}{D_{min} + 2}\frac{2}{3\cos^2\alpha - 1} \qquad \Psi = \psi + 90° \tag{13b}$$

RESULTS AND DISCUSSION

The change of molecular orientation at the fiber end in the early stage of uniaxially drawing process is visualized in Figure 4 as the image of (a) in-plane orientation function and (b) orientation azimuth angle, calculated with eq 13b at 720 cm^{-1} (CH_2 rocking[47,48]) under an assumption of $\alpha = 90°$, before and after applying tensile strain. In the image of orientation function (Figures 4a-1 and 4a-2), the in-plane orientation function at the fiber end does not change clearly before and after applying tensile strain. On the other hand, the orientation azimuth angle calculated at 720 cm^{-1} shows a few more change in the matrix. Before stretching (Figure 4b-1), the random values are seen in the pixels

dx.doi.org/10.1021/ma2003129 |*Macromolecules* 2011, 44, 3950–3957

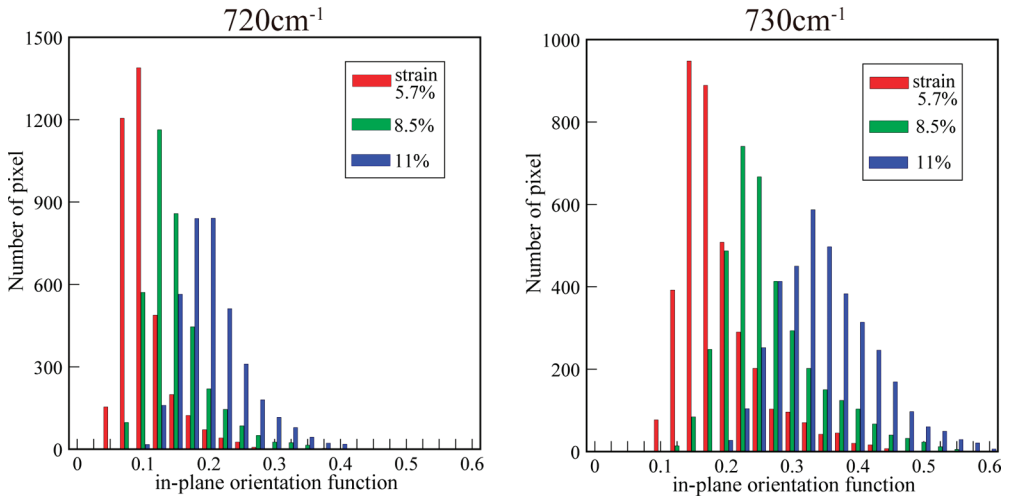

Figure 6. Image histograms of in-plane orientation function in a 350 μm × 400 μm rectangular area which is centered at the fiber end. The histograms are calculated at (left) 720 and (right) 730 cm^{-1} absorption bands and at (red) 5.7, (green) 8.5, and (blue) 11% tensile strain, respectively.

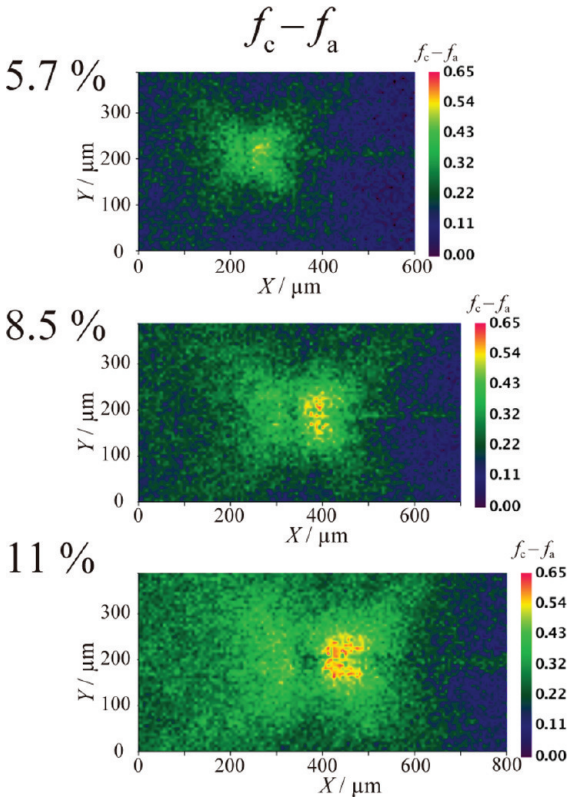

Figure 7. Subtraction image of the in-plane orientation function of crystalline and amorphous region calculated from 720 and (right) 730 cm^{-1} with eqs 14 at (upper) 5.7, (middle) 8.5, and (lower) 11% tensile strain.

of the matrix, and the green area (0°) is seen only on the fiber area in which the molecular orientation of the fiber exists. After applying 2.9% tensile strain (Figure 4b-2) the area of the green color increases in the matrix. Thus, the orientation axis becomes parallel to the drawing direction in the matrix with applying tensile strain. In order to analyze this change quantitatively, the image histogram of Figure 4b-1) (blue bar) and Figure 4b-2) (red bar) is shown in Figure 4c. The *x*-axis corresponds to the value of orientation azimuth angle, and the *y*-axis corresponds to the number of pixels, which is proportional to the area size. The histogram shows the random variation at 0% strain, whereas at strain 2.9% the 0° has the maximum frequency with the variation of ±20°. The numbers of pixels whose azimuth angle is in the range of 0°−5° increases from 195 (at 0% strain) to 677 (at 2.9% strain). The results indicate that the distribution of orientation azimuth angle detects a small change of molecular orientation in the early stage of drawing, which is not detected only with the visualization of orientation function.

The in-plane orientation functions calculated from two absorption bands, 720 and 730 cm^{-1}, are displayed in Figure 5 at tensile strain, 5.7, 8.5, and 11%. The absorbance band was assigned to CH_2 rocking, in which the crystalline region contributes to the band at 730 cm^{-1} and both the crystalline and amorphous regions contribute to 720 cm^{-1}.[47,48] At the fiber end, a characteristic localized change of matrix orientation is clearly observed. The local high orientation area around the fiber end corresponds to the stress concentration, and the area expands and the magnitude of the in-plane orientation function increases with increasing the tensile strain. Alongside the fiber, the random orientation is kept in the matrix polyethylene. The localized stress concentration image at the fiber end at 730 cm^{-1} can be observed in the more expanded area than at 720 cm^{-1}. The magnitude of in-plane orientation function at 730 cm^{-1} is higher than that at 720 cm^{-1} in each tensile strain. For the analysis of relationship between the tensile strain and the magnitude of in-plane orientation function, the image histogram of the orientation function at 720 and 730 cm^{-1} in each tensile strain is shown in Figure 6. It is calculated from the pixels in a 350 μm × 400 μm rectangular area whose center corresponds to the fiber end. The histogram becomes broader with increasing the tensile strain. This means the unevenness of matrix orientation increases. The maximum frequency of histogram shifts from 0.10 to 0.20 at 720 cm^{-1} and from 0.15 to 0.33 at 730 cm^{-1} with increasing tensile strain. The higher value of orientation function at 730 cm^{-1} indicates that the crystalline region of polyethylene contributes to the orientation function than the amorphous region in the earlier stage of the drawing process. This difference has been explained by the faster relaxation of amorphous regions than crystalline regions.[52−54]

dx.doi.org/10.1021/ma2003129 |*Macromolecules* 2011, 44, 3950–3957

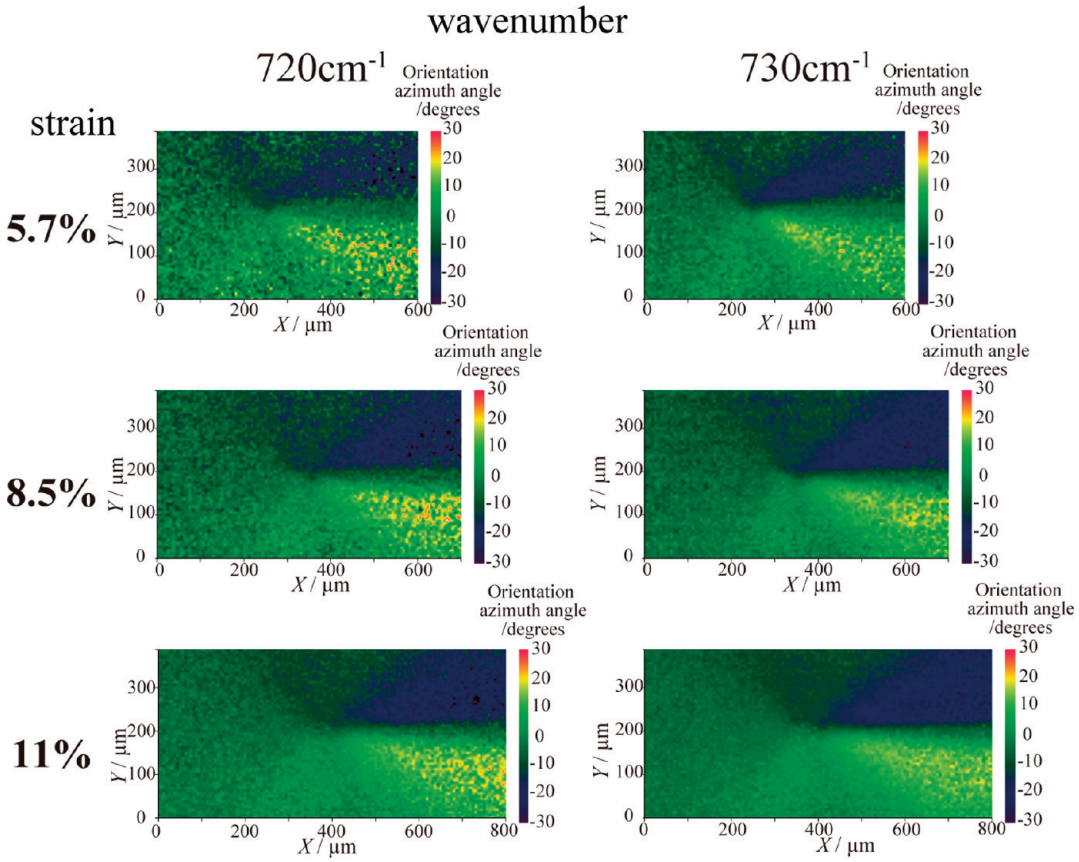

Figure 8. Images of the orientation azimuth angle calculated at (left) 720 and (right) 730 cm^{-1} in the polyethylene fiber composite film at (upper) 5.7, (middle) 8.5, and (lower) 11% tensile strain.

The subtraction image of the in-plane orientation function of crystalline and amorphous region is displayed in Figure 7 calculated with the equation

$$f_c - f_a = \frac{f_{730} - f_{720}}{1 - \chi_c} \tag{14a}$$

where χ_c is the crystallinity defined as

$$\chi_c = \frac{A_{730}}{A_{720}} \tag{14b}$$

and f_c and f_a are the orientation function of the CH_2 rocking in the crystalline and amorphous region, respectively. With increasing the tensile strain, the subtracted values in the stress concentrated area increases except for the center area near the fiber end in the matrix especially at 11% tensile strain. Comparing with the f_c (f_{730}) image in Figure 5, the inhomogeneous distribution in the subtracted image at the fiber end indirectly suggests a kind of difference in the deformation process of molecules in crystalline and amorphous regions just prior to the plastic deformation.

In Figure 8, the images of orientation azimuth angles are shown at tensile strain, 5.7, 8.5, and 11% calculated from two absorption bands at 720 and 730 cm^{-1}. Alongside the fiber, about ±15° of the orientation azimuth angles (yellow (−15°) and blue area (+15°)) are clearly visualized. On the other hand, in the left side of the fiber end, the inclination can be seen but in the smaller area, and the green area (0°) is widely seen with random noise. The similar shape of the distribution pattern of orientation azimuth angle is observed at each tensile strain. The random noise decreases and the image becomes sharp with increasing tensile strain in Figure 8.

The shape of distributions of in-plane orientation function and orientation azimuth angle is explained by the stress distribution in the short fiber reinforced composite material. When it is uniaxially drawn along the fiber, the matrix stress is transferred to the fiber by the interfacial shear stress, particularly near the fiber ends.[49−51] Therefore, the stress concentration near the fiber end induces the local high orientation in Figure 5 and the inhomogeneous subtraction values of $f_c - f_a$ in Figure 7. Alongside of the fiber, the applied tensile stress to the matrix becomes very small and the shear stress is applied, because the tensile stress is applied to the fiber due to the stress transfer from the matrix to the fiber. Thus, in this area, the low orientation of matrix polyethylene (in Figure 5) and the inclination of the direction of orientation axis from the drawing direction (in Figure 8) are observed. On the other hand, at the left side of the fiber end, the matrix polyethylene is deformed only by the tensile strain, which is larger than that of alongside the fiber. The distribution of orientation azimuth angle around the fiber end is very similar to the isoclinic fringe pattern in the photoelastic study.[49]

Figure 9 shows the images of (upper) in-plane orientation function and (lower) orientation azimuth angle at 1464 and 1470 cm^{-1} (CH_2 bending,[4748]) under an assumption of α = 90°, measured at 11% tensile strain. The images of orientation azimuth angle at 1464 and 1470 cm^{-1} are very similar to those at 720 and 730 cm^{-1} (shown in Figure 8). It suggests that the orientation azimuth angle does not depend on the absorption bands. On the

dx.doi.org/10.1021/ma2003129 |*Macromolecules* 2011, 44, 3950–3957

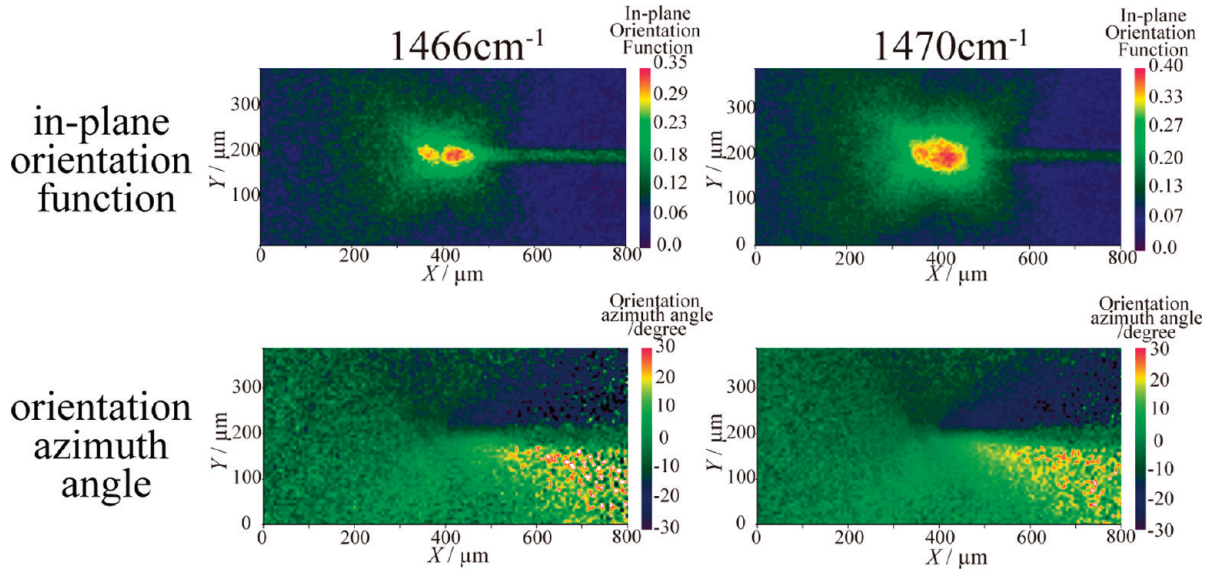

Figure 9. Images of (upper) in-plane orientation function and (lower) orientation azimuth angle calculated at (left) 1464 and (right) 1470 cm^{-1} in the polyethylene fiber composite film at 11% tensile strain.

other hand, the image of in-plane orientation function is different among each absorption band. There are some reasons of this difference, for example, the different contribution of crystalline and amorphous region to the in-plane molecular orientation and the difference of spatial resolution among absorption bands. The pixel size of using instrument is 6.25 μm, which is near to the wavelength of using absorption band, and the spatial resolution has a dependence of wavelength of using infrared radiation.

CONCLUSION

The distributions of in-plane orientation function and orientation azimuth angle are calculated from the absorbance images measured with a linear polarizer with four different angles. This analytic method is applied to visualize the local deformation of matrix polyethylene near the fiber end in the uniaxially drawn LDPE/PE fiber composite film. The distribution of orientation azimuth angle detects a small change of molecular orientation in the early stage of drawing process. In the later stage, the orientation azimuth angle visualizes the contribution of shear stress to the deformation of the matrix around the fiber end. The stress concentration at the fiber end is shown in the distribution of in-plane orientation function. From a comparison of in-plane orientation function calculated from the band assigned to CH_2 rocking, the molecular orientation in the crystalline region occurs earlier than in the amorphous region in the early stage of drawing.

By introducing the subtraction image of f_c and f_a, the method enables to visualize the different contribution from the crystalline and amorphous regions to the localized molecular orientation that is induced in the locally stress-concentrated area at the fiber end of the matrix, just prior to the plastic deformation in the drawing process. Such kinds of information are first observed using the imaging method with the algorithm in this study, which will be useful to analyze the localized variation of molecular orientation of macromolecular systems.

REFERENCES

(1) Lewis, E. N.; Treado, P. J.; Reedor, R. C.; Stay, G. M.; Dowrey, A. E.; Marcott, C.; Levin, I. W. *Anal. Chem.* **1995**, *67*, 3377.
(2) Koenig, J. L.; Wang, S. Q.; Bhargava, R. *Anal. Chem.* **2001**, *73*, 360 A.
(3) Hashimoto, Y.; Ishiaku, U. S.; Leong, Y. W.; Hamada, H.; Tsujii, T. *Polym. Eng. Sci.* **2006**, *46*, 205.
(4) Ribar, T.; Bhargava, R.; Koenig, J. L. *Macromolecules* **2000**, *33*, 8842.
(5) Ribar, T.; Koenig, J. L. *Macromolecules* **2001**, *34*, 8840.
(6) Miller-Chou, B. A.; Koenig, J. L. *Macromolecules* **2002**, *35*, 440.
(7) González-Benito, J.; Koenig, J. L. *Macromolecules* **2002**, *35*, 7361.
(8) Miller-Chou, B. A.; Koenig, J. L. *Macromolecules* **2003**, *36*, 4851.
(9) Snively, C. M.; Koenig, J. L. *Macromolecules* **1998**, *31*, 3753.
(10) Bhargava, R.; Wang, S. Q.; Koenig, J. L. *Macromolecules* **1999**, *32*, 2748.
(11) Snively, C. M.; Koenig, J. L. *J. Polym. Sci., Part B: Polym. Phys.* **1999**, *37*, 2261.
(12) Rafferty, D. W.; Koenig, J. L.; Magyar, G.; West, J. L. *Appl. Spectrosc.* **2002**, *56*, 284.
(13) Mavrich, A. M.; Ishida, H.; Koenig, J. L. *Appl. Spectrosc.* **1995**, *49*, 149.
(14) González-Benito, J. *J. Colloid Interface Sci.* **2003**, *267*, 326.
(15) Biswal, D.; Hilt, J. Z. *Polymer* **2006**, *47*, 7355.
(16) Biswal, D.; Hilt, J. Z. *Macromolecules* **2009**, *42*, 973.
(17) Sorber, J.; Steiner, G.; Schulz, V.; Guenther, M.; Gerlach, G.; Salzer, R.; Arndt, K. F. *Anal. Chem.* **2008**, *80*, 2957.
(18) Vogel, C.; Wessel, E.; Siesler, H. W. *Biomacromolecules* **2008**, *9*, 523.
(19) Vogel, C.; Wessel, E.; Siesler, H. W. *Macromolecules* **2008**, *41*, 2975.
(20) Oh, S. J.; Koenig, J. L. *Anal. Chem.* **1998**, *70*, 1768.
(21) Chalmers, J. M.; Everall, N. J.; Schaeberle, M. D.; Levin, I. W.; Lewis, E. N.; Kidder, L. H.; Wilson, J.; Crocombe, R. *Vib. Spectrosc.* **2002**, *30*, 43.
(22) Chernev, B.; Belegratis, M. R.; Ingolic, E. *Macromol. Symp.* **2008**, *265*, 272.
(23) Yamaguchi, S.; Leong, Y. W.; Tsujii, T.; Mizoguchi, M.; Ishiaku, U. S.; Hamada, H. *J. Appl. Polym. Sci.* **2005**, *98*, 294.
(24) Rhuday, K. L.; Su, S.; Howell, H. R.; Urban, M. W. *Langmuir* **2008**, *24*, 1808.
(25) Sommer, A. J.; Tisinger, L. G.; Marcott, C.; Story, G. M. *Appl. Spectrosc.* **2001**, *55*, 252.
(26) Gupper, A.; Wilhelm, P.; Schmied, M.; Kazarian, S. G.; Chan, K. L. A.; Reussner, J. *Appl. Spectrosc.* **2002**, *56*, 1515.

(27) Patterson, B. M.; Havrilla, G. J. *Appl. Spectrosc.* **2006**, *60*, 1256.
(28) Kazarian, S. G.; Chan, K. L. A. *Appl. Spectrosc.* **2010**, *64*, 135A.
(29) Chan, K. L. A.; Kazarian, S. G. *Appl. Spectrosc.* **2003**, *57*, 381.
(30) Kazarian, S. G.; Chan, K. L. A. *Macromolecules* **2004**, *37*, 579.
(31) Fleming, O. S.; Chan, K. L. A.; Kazarian, S. G. *Vib. Spectrosc.* **2004**, *35*, 3.
(32) Fleming, O. S.; Chan, K. L. A.; Kazarian, S. G. *Polymer* **2006**, *47*, 4649.
(33) Kazarian, S. G.; Chan, K. L. A. *Macromolecules* **2003**, *36*, 9866.
(34) Van der Weerd, J.; Chan, K. L. A.; Kazarian, S. G. *Vib. Spectrosc.* **2004**, *35*, 9.
(35) Van der Weerd, J.; Kazarian, S. G. *J. Controlled Release* **2004**, *98*, 295.
(36) Jamshidi, M. M.; Vij, J. K.; Nguyen, H. T. *Ferroelectrics* **2002**, *277*, 229.
(37) Nge, T. T.; Hori, N.; Takemura, A.; Ono, H.; Kimura, T. *J. Appl. Polym. Sci.* **2003**, *90*, 1932.
(38) Vogel, C.; Wessel, E.; Siesler, H. W. *Appl. Spectrosc.* **2008**, *62*, 599.
(39) Vogel, C.; Hoffmann, G. G.; Siesler, H. W. *Vib. Spectrosc.* **2009**, *49*, 284.
(40) Snively, C. M.; Koenig, J. L. *J. Polym. Sci., Part B: Polym. Phys.* **1999**, *37*, 2353.
(41) Wang, W.; Jin, Y.; Yang, X.; Su, Z. *J. Polym. Sci., Part B: Polym. Phys.* **2010**, *48*, 541.
(42) Merten, C.; Kowalik, T.; Asshoff, S. J.; Hartwig, A. *Macromol. Chem. Phys.* **2010**, *211*, 1627.
(43) Harada, M.; Morimoto, M.; Ochi, M. *J. Appl. Polym. Sci.* **2003**, *87*, 787.
(44) Hermans, P. H.; Platzek, P. *Kolloid-Z.* **1938**, *88*, 68.
(45) Ward, I. M. *Structure and Properties of Oriented Polymers*; Chapman & Hall: London, 1997.
(46) Zbinden, R. *Infrared Spectroscopy of High Polymers*; Academic Press: New York, 1964.
(47) Krimm, S.; Liang, C. Y.; Sutherland, G. B. B. M. *J. Chem. Phys.* **1956**, *25*, 549.
(48) Read, B. E.; Stein, R. S. *Macromolecules* **1968**, *1*, 116.
(49) Tyson, W. R.; Davies, G. J. *Br. J. Appl. Phys.* **1965**, *16*, 199.
(50) Song, D. Y.; Takeda, N.; Shioya, T.; Nakata, K. *Polym. Compos., Part A* **1996**, *27*, 357.
(51) Zhao, Q.; Frogley, M. D.; Wagner, H. D. *Adv. Technol.* **2002**, *13*, 759.
(52) Seguela, R.; Rietsch, F. *Polymer* **1986**, *27*, 532.
(53) Pazur, R. J.; Ajji, A.; Prud'homme, R. E. *Polymer* **1993**, *34*, 4004.
(54) Butler, M. F.; Donald, A. M.; Ryan, A. J. *Polymer* **1998**, *39*, 39.